Journal of Catalysis **211,** 470–481 (2002)
doi:10.1006/jcat.2002.3754

Characterization and Comparison of the Activity of Boron-Modified Co/TiO_2 Catalysts in Butan-2-ol Conversion and Oxidative Dehydrogenation of Ethane

Younes Brik,*,† Mohamed Kacimi,* François Bozon-Verduraz,† and Mahfoud Ziyad*,[1]

*Faculté des Sciences, Département de Chimie, Laboratoire de Physico-chimie des Matériaux et Catalyse, Avenue Ibn Battouta, B.P. 1014, Rabat, Morocco; and †Laboratoire de Chimie des Matériaux Divisés et Catalyse, Université Paris 7, 2 place Jussieu, 75251 Paris Cedex, France

Received April 17, 2002; revised July 18, 2002; accepted July 18, 2002

Cobalt- and cobalt–boron-loaded TiO_2 (anatase) catalysts were prepared and characterized before and after catalytic tests by XRD, HRTEM, IR, UV–visible, and laser Raman spectroscopy. Their activity was investigated in oxidative dehydrogenation (ODH) of ethane. In the absence of boron, the best performances were exhibited by the sample containing 7.6 wt% Co, which was selected for further investigations. At 550°C, it displayed a stationary state with a conversion of 22.2% and an ethylene selectivity around 60%. This catalyst also showed in the first 3 h on stream a 30% decay in activity that was attributed to a concomitant loss of specific surface area and the formation of $CoTiO_3$ and Co_2TiO_4 phases. The addition of 0.25 wt% boron to this $Co(7.6)/TiO_2$ sample improved the ethane conversion and the ethylene selectivity, which attained 28.4 and 67%, respectively. Boron concentrations superior to 0.25 wt% negatively affected the catalysts performances, probably because at high loadings it profoundly modified the acid–base properties of the surface. XRD and HRTEM analyses showed that at the same time the size of Co_3O_4 crystallites decreased. IR investigations confirmed the increase in acidity upon boron addition and the decrease in strength of the basic sites which were involved in the dehydrogenation processes.

The catalytic behavior and the acid–base properties of $Co(7.6)/TiO_2$ loaded with different amounts of boron were also studied using butan-2-ol conversion. Boron addition enhanced the dehydration and the dehydrogenation reactions. However, above 0.25 wt% it decreased the dehydrogenation activity, confirming the modifications of the properties of the acid–base centers revealed by the IR studies. For this optimal concentration of boron, the activity and the selectivity in butan-2-ol dehydrogenation exhibited a maximum that coincided with the one observed in the ethane ODH, which suggests that both reactions possibly involved the same type of active centers.

Key Words: **ethane oxidative dehydrogenation; cobalt/TiO_2 catalysts; cobalt–boron/TiO_2 catalysts; UV–visible; IR; HRTEM; laser Raman spectroscopy.**

1. INTRODUCTION

Partial oxidation and oxidative dehydrogenation of light alkanes have been intensively studied in the last decade for their promising commercial possibilities and also for the academic challenge they represent. However, until now, except for butane oxidation into maleic anhydride, there have been no large-scale industrial operations for these processes, probably because the yields are not yet satisfactory. The presence of O_2 in the reaction mixture restrains the thermodynamic limitations but conversely reduces the stability of the valuable products. Therefore, it seems that the problem resides essentially in finding a catalyst that allows a lowering of the reaction temperature while preserving acceptable performances. Many types of solids have been tested, including mixtures of transition metal oxides dispersed on large specific surface area carriers (1, 2). Pure phases such as perovskites, $Mg_3(VO_4)_2$, phosphates, and heteropolyoxometallates of Keggin or Dawson containing redox metals such as V, Mo, W, Ga, Cu, Fe, and Cr, were also investigated (3–6). The literature has reported several reasonable conversions often achieved when N_2O is used as the oxygen source or under severe conditions at the expense of the selectivity. Introduction of promoters such as alkalis (7), phosphorus (8–10), or boron (11, 12) has also been investigated and numerous studies showed that modifying the acid–base and the morphological properties of the system might increase the activity as well as the selectivity.

In a previous work, it was shown that Co-loaded TiO_2 (anatase), usually used in hydrogenation processes and Fischer–Tropsch reactions, is quite active in ethane ODH (13). The catalyst exhibits optimal performances when the cobalt content is around 7.6 wt%. At 550°C, the global conversion reaches 22.2% with an ethylene selectivity of 60%. For loadings superior to 7.6 wt%, the activity and selectivity decrease, probably because the size of Co_3O_4 crystallites increases and enhances the total oxidation of C_2H_6. On the other hand, the $Co(7.6)/TiO_2$ sample undergoes in the first 3 h of reaction a deactivation which is accompanied by the

[1] To whom correspondence should be addressed. Fax: (212) 37 77 54 40. E-mail: ziyad@fsr.ac.ma.

0021-9517/02 $35.00

formation of $CoTiO_3$ and Co_2TiO_4 phases (13). This catalyst rebuilding modifies the surface composition, changes the Co^{2+}/Co^{3+} ratio, and lowers the specific surface area. Cobalt-containing materials were also frequently used in oxidation reactions, but it has always been difficult to correlate their activity to a redox mechanism since the oxidation of Co^{2+} ions is not easily achieved in conventional conditions. Thus, the activity is often related to oxygen-adsorbed species on the catalyst surface which are assumed to intervene in the alkane activation.

The current work is an extension of previous studies performed on cobalt-loaded TiO_2 in ethane ODH reactions (13). Its main goal is to improve the catalytic abilities of the system and determine the impact of boron addition on the activity of cobalt species. In fact, it has been claimed that on B_2O_3/Al_2O_3 at 550°C, the activity reaches 38%, with an ethylene selectivity of 58% when using O_2 (12). Boron oxides do not have redox properties and, therefore, the reaction mechanism is certainly not of Mars and van Krevelen type. The addition of boron (as H_3BO_3) to a Co/TiO_2 Fisher–Tropsch catalyst also proved to have a beneficial effect on the reducibility of the active phase and on the CO hydrogenation (15).

The behavior of Co/TiO_2 and $B–Co/TiO_2$ systems is not yet well understood and has hardly been investigated in ODH reactions. The present study is concerned with the determination of the performances of boron-modified $Co(7.6)/TiO_2$ in the ethane ODH. Special attention is devoted to the characterization of the catalysts before and after the catalytic runs using diffuse reflectance spectroscopy, laser Raman spectroscopy, and HRTEM measurements. The acid–base properties of the catalysts upon boron addition is examined by FTIR, adsorbing and desorbing 2,6-dimethylpyridine (2,6-lutidine or C_7H_9N) at different temperatures. Butan-2-ol conversion is also studied in order to (i) compare the catalysts dehydrogenation activity in this reaction with that of ethane ODH and (ii) correlate the acid–base properties of the solids to their activity in both reactions (16).

2. EXPERIMENTAL

2.1. Catalysts Preparation

The synthesis of $B(x)Co(7.6)/TiO_2$ samples that contain different amounts of boron and 7.6 wt% cobalt was carried out using the coimpregnation and the sequential impregnation methods. The titania in its anatase form was supplied by Rhône–Poulenc (TiO_2 DT51) and used without any further treatment. Chemical determination of its composition revealed that it contains less than 4–5% sulfates, resulting from its precipitation in sulfuric acid media. The cobalt and boron loadings were performed using titrated solutions of $Co(NO_3)_2 \cdot 6H_2O$ and H_3BO_3. They were added simultaneously or sequentially to TiO_2. The resulting mixture was maintained under stirring at 80°C until the water completely evaporated. The recovered solids were dried at 120°C, then calcined in a rotating furnace for 4 h at 550°C under flowing air (30 $cm^3\ min^{-1}$). The catalysts prepared by coimpregnation are labeled $B(x)Co(7.6)/TiO_2$, where x ($0 \le x \le 2$) represents the weight percent of boron. Those prepared by sequential impregnation are named $B(x)/Co(7.6)/TiO_2$.

2.2. Characterization Techniques

The specific surface areas of the samples, which were evacuated for 2 h at 300°C, were measured before and after the catalytic tests. Nitrogen adsorption at −196°C and a Micromeritics apparatus were used. The results are displayed in Table 1. They show that loading $TiO_2$with cobalt decreases the specific surface areas of the samples. Boron addition to $Co(7.6)/TiO_2$ minimizes this loss. The catalysts synthesized by sequential impregnation exhibit slightly lower surface areas than those prepared by coimpregnation.

TABLE 1

Specific Surface Areas before and after Catalytic Tests: Chemical Analysis of the Samples

Sample	Surface before catalysis ($m^2\ g^{-1}$)	Surface after catalysis ($m^2\ g^{-1}$)	Chemical analysis			
			Co/Ti		B/Co	
			Theoretical	Observed	Theoretical	Observed
TiO_2	89	81.2	—	—	—	—
$Co(7.6)/TiO_2$	63.5	40.7	7.6	7.6	—	—
$B(0.2)Co(7.6)/TiO_2$	69.2	43.1	7.6	7.6	2.6×10^{-2}	2.5×10^{-2}
$B(0.25)Co(7.6)/TiO_2$	75.9	49.7	7.6	7.5	3.3×10^{-2}	3.2×10^{-2}
$B(0.25)/Co(7.6)/TiO_2$	64.2	46.6	7.6	7.6	3.3×10^{-2}	3.3×10^{-2}
$Co(7.6)/B(0.2)/TiO_2$	69.8	48.1	7.6	7.5	3.3×10^{-2}	3.1×10^{-2}
$B(0.33)Co(7.6)/TiO_2$	69.9	52.3	7.6	7.5	4.3×10^{-2}	4.4×10^{-2}
$B(0.5)Co(7.6)/TiO_2$	69.3	51.1	7.6	7.5	6.6×10^{-2}	6.5×10^{-2}
$B(1)Co(7.6)/TiO_2$	69.7	62.6	7.6	7.6	13.2×10^{-2}	13.1×10^{-2}
$B(2)Co(7.6)/TiO_2$	69.9	64.9	7.6	7.6	26.3×10^{-2}	26.4×10^{-2}

Chemical analyses were carried out at the Central Service of analysis (CNRS–Vernaison) by inductive coupling plasma–atomic emission spectroscopy (ICP–AES). The results are reported in Table 1. They show that the amounts of Co and B found in the samples are in agreement with the theoretical values. No significant sublimation of boron was observed even after a calcination at 550°C.

X-ray powder diffraction patterns were recorded with a Siemens D5000 high-resolution spectrometer using Cu $K\alpha$ radiation ($\lambda = 1.540598$ Å). The data were collected with a step of 0.02° (2θ) at room temperature.

Laser Raman spectra were obtained in backscattering geometry with a Dilor XY spectrometer using the 514.5-nm excitation line of a coherent argon Spectra Physics Laser model 165. The data were collected keeping the power under 20 mW. The spectrometer was also equipped with a monochromator utilized in the subtractive mode to select a given range. The detector used was a multichannel Jobin–Yvon 1024* 256 CCDS matrix, which is thermoelectrically cooled.

HRTEM micrographs were taken using a JEOL 100CXII microscope operating at 100 kV. The catalyst was ultrasonically dispersed in ethanol, and the suspension was deposited on a copper grid coated with a porous carbon film and then allowed to dry.

FTIR transmission spectra were recorded on Perkin–Elmer 1730 and Bruker Equinox spectrometers (resolution 4 cm^{-1}, 50 scans). The samples were pressed into self-supporting disks (about 25 mg/cm^2) and placed in a stainless-steel cell (In Situ Research Instruments) that allows *in situ* analysis. Lutidine adsorption–desorption experiments were performed in the 20–500°C range.

Diffuse reflectance spectra were recorded with 300 mg of the sample at room temperature between 190 and 2500 nm on a Varian Cary 5E spectrometer equipped with a double monochromator and an integration sphere coated with polytetrafluoroethylene (PTFE). PTEF was used as a reference.

2.3. Catalytic Tests

Catalytic behavior and acid–base properties of the samples were measured using butan-2-ol conversion as the probe reaction. The runs were performed at 200°C in a dynamic microreactor containing, between two quartz wool plugs, 100 mg of catalyst sieved to 125–180 μm. Prior to reaction the catalysts were evacuated at 400°C. The alcohol was diluted in pure nitrogen or air and supplied to the reactor at a partial pressure of 8.3×10^2 Pa. The total flow rate of the reaction mixture was 60 $cm^3\ min^{-1}$.

Ethane ODH was carried out in a quartz U-shaped continuous-flow microreactor operated at atmospheric pressure. Prior to the reaction the catalyst was sieved to a grain size ranging from 125 to 180 μm, then set into the reactor between two quartz wool plugs and pretreated with a pure nitrogen stream. The reaction mixture was composed of 6 vol% ethane, 3 vol% O_2, and 91 vol% N_2 in a total flow rate of 60 $cm^3\ min^{-1}$. Analyses of the effluent gases were performed using two online chromatographs: a FID for hydrocarbon separation on a Porapak Q column and another one equipped with catharometers and a silica gel column for the oxygenated products. Under the selected experimental conditions the reaction started around 300°C and produced only ethylene and CO_x.

3. RESULTS

3.1. Catalysts Characterization before the Catalytic Tests

XRD patterns. The X-ray diffraction patterns of $Co(7.6)/TiO_2$ show that besides the titanium dioxide, there are additional peaks attributed to crystallites of Co_3O_4 (Table 2). This formation of Co_3O_4 might be attributed to the fact that the sample contains more cobalt than the amount needed for the completion of a monolayer. The excess is transformed, in oxidative atmospheres, into Co_3O_4. The formation of this monolayer of cobalt is not the limiting factor that determines the performances of the catalyst. The interactions between the loaded element and the carrier play perhaps a more important role because in many cases they modify the original behavior of the supported metal. In order to picture these interactions, the crystallographic features of TiO_2 (anatase) have to be taken into account (14).

Table 2 summarizes the results of X-ray diffraction patterns of $B(x)Co(7.6)/TiO_2$ and shows that boron addition did not affect the structure of TiO_2, albeit it decreases the relative intensities of Co_3O_4 diffraction peaks. Concomitantly, it lowers the size of Co_3O_4 crystallites (Table 2). Other than the Co_3O_4 no mixed compound containing Co–B was detected. The $B(x)Co(7.6)/TiO_2$ samples loaded with more than 1% B did not show any crystalline phase except TiO_2 (anatase). These results suggest that boron modifies the crystalline growth of Co_3O_4, in agreement with what was reported in the literature for B–Co/TiO_2 and B–Co/Al_2O_3 systems (15, 17).

TABLE 2

X-Ray Analysis of the Samples before Catalysis and the Size of Co_3O_4 Crystallites

Sample	Detected phases	Size of Co_3O_4 crystallites (nm)
$Co(7.6)/TiO_2$	TiO_2 anatase + Co_3O_4	17.9
$B(0.25)Co(7.6)/TiO_2$	TiO_2 anatase + Co_3O_4	19.2
$B(0.33)Co(7.6)/TiO_2$	TiO_2 anatase + Co_3O_4	17.1
$B(0.5)Co(7.6)/TiO_2$	TiO_2 anatase + Co_3O_4	16.5
$B(1)Co(7.6)/TiO_2$	TiO_2 anatase	—
$B(2)Co(7.6)/TiO_2$	TiO_2 anatase	—

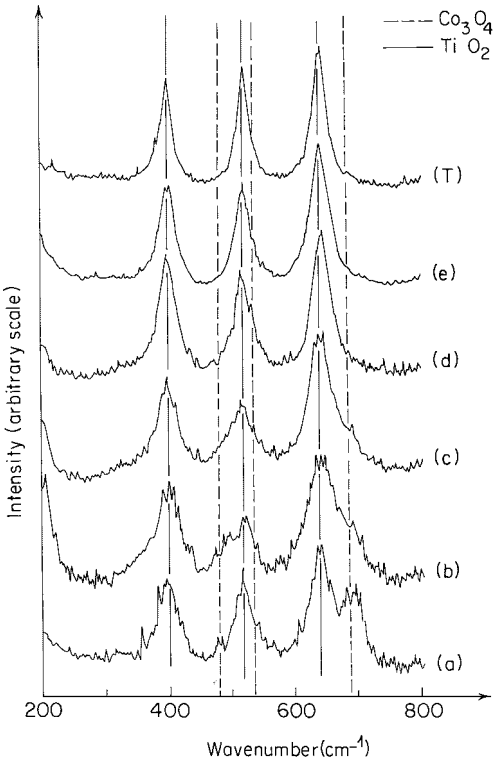

FIG. 1. Raman spectra of B(x)Co(7.6)/TiO_2: (a) Co(7.6)/TiO_2, (b) B(0,25)Co(7.6)/TiO_2, (c) B(0.5)Co(7.6)/TiO_2, (d) B(1)Co(7.6)/TiO_2, (e) B(2)Co(7.6)/TiO_2, and (T) TiO_2.

Laser Raman spectroscopy. Laser Raman spectra of the samples are compared on Fig. 1. Titanium oxide is characterized by three bands, located at 397, 514, and 640 cm^{-1} (spectrum T). The bands at 397 and 640 cm^{-1} are assigned to B_{1g} and E_{1g} modes, respectively, while the band at 640 cm^{-1} is a doublet of A_{2g} and B_{1g} modes (18). Loading TiO_2 with 7.6 wt% cobalt gives rise to a new absorption near 692 cm^{-1} and two shoulders, at 485 and 524 cm^{-1}, assigned to the A_{1g}, E_g, and F_{2g} active Raman modes of the direct spinel Co_3O_4, respectively (19, 20). The addition of boron to the system produces, in agreement with the XRD results, a decrease in the intensity of Co_3O_4 bands. When the boron content reaches 1 wt%, Co_3O_4 vibrations disappear completely (spectra d and e). Boron oxide B_2O_3 normally displays two absorptions, located around 806 and 602 cm^{-1}, while boric acid exhibits two intense peaks, at 880 and 500 cm^{-1} (21). None of these bands was identified on the spectra, probably because boron leads to a formation on the TiO_2 surface of amorphous compounds not detectable by this technique (19).

TEM and HRTEM studies. Transmission electron microscopy (TEM) observation of the samples showed that TiO_2 particles are almost spherical or slightly stretched. Their size varies between 20 and 30 nm, in agreement with the results of Roy *et al.* (22). However, by this (TEM) technique it was impossible to distinguish TiO_2 particles from those of Co_3O_4, due to the small difference in size and the poor contrast between them.

The high-resolution TEM (HRTEM) investigations (Figs. 2A and 2B) revealed that some of the particles are covered with parallel fringes. Measurement of the distance separating two consecutive fringes on the (a), (b), and (c) particles allows the identification of crystallographic planes of TiO_2 and Co_3O_4 crystallites. On particle (a) this distance is equal to 3.56 Å. This can reasonably be attributed to the interplanar spacing of (101) planes of TiO_2 anatase, which are the preferentially exposed ones. Theoretically, this spacing is $d(101) = 3.51$ Å (23). On (b) and (c) particles the distances between the fringes are smaller and equal to $d(b) = 2.51$ Å and $d(c) = 2.42$ Å. They can be assigned to the d-spacing of (311) planes in Co_3O_4 spinel. The size of particle (b), which corresponds to Co_3O_4, is 19 nm. This value is close to the one previously determined by XRD (17.9 nm)

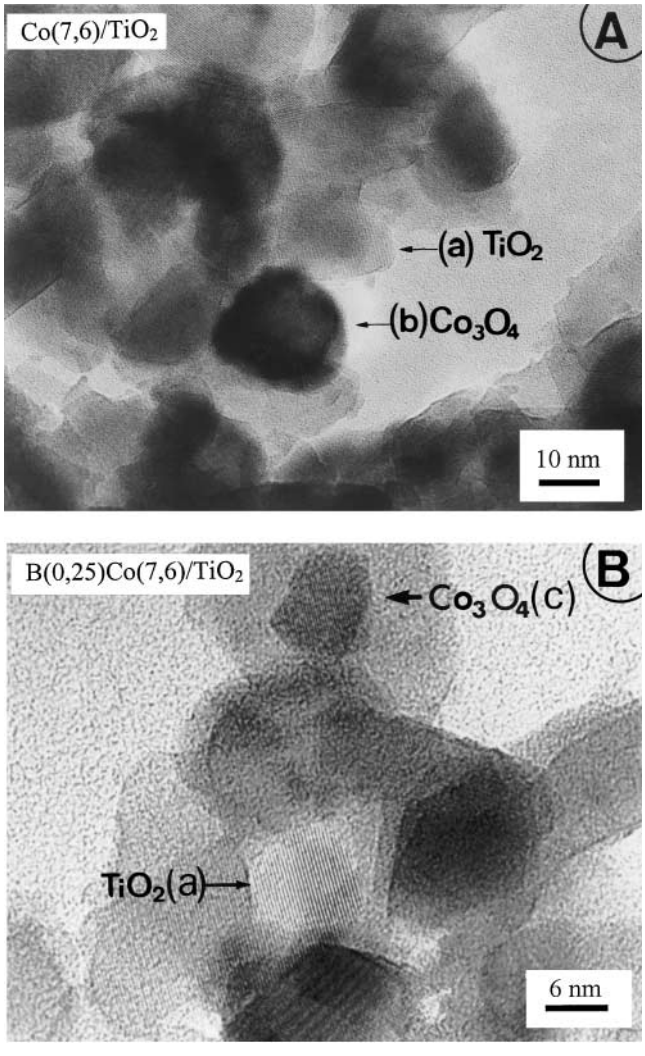

FIG. 2. HRTEM micrographs of B(x)Co(7.6)/TiO_2.

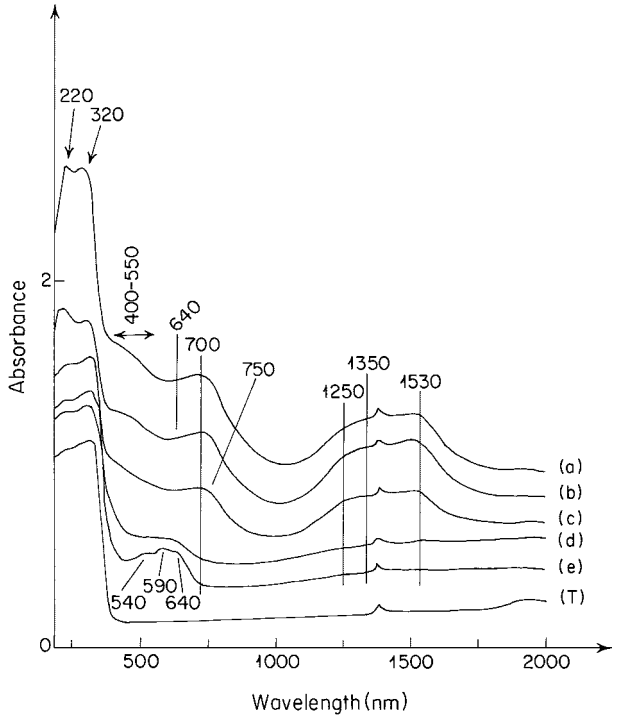

FIG. 3. DR Spectra of B(x)Co(7,6)/TiO_2: (a) Co(7.6)/TiO_2, (b) B(0.25)Co(7.6)/TiO_2, (c) B(0.5)Co(7.6)/TiO_2, (d) B(1)Co(7.6)/TiO_2, (e) B(2)Co(7.6)/TiO_2, and (T) TiO_2.

(Table 1). Boron addition to Co(7.6)/TiO_2 was found to significantly decrease the dimensions of Co_3O_4 particles. For the B(0.25)Co(7.6)/TiO_2 sample (Fig. 2B), particles with sizes around 7 nm were detected.

UV–visible NIR DRS. The diffuse reflectance spectra reported in Fig. 3 show that all the samples display a strong absorption in the UV range due to TiO_2 interband transitions (valence band → conduction band). The maxima appearing at 320 and 220 nm are attributed to $O^{2-} \rightarrow Ti^{4+}$ charge transfer bands. In the visible region there is a broad band near 700 nm, a weak shoulder at 640 nm, and a more pronounced one between 400 and 550 nm. In the NIR we observe a set of overlapping bands centered on 1250, 1350, and 1530 nm. Most of these bands can be ascribed to Co^{2+} ions hosted by tetrahedral sites (24). There is also, around 1380 nm, a sharp band 2ν(OH) due to the harmonic absorption of residual hydroxyl groups. The bands located at 640 nm and 1250, 1350, 1530 nm are associated with ν_1 and ν_2 absorptions that result from the transitions $^4A_2(F) \rightarrow {}^4T_1(F)$ and $^4A_2(F) \rightarrow {}^4T_1(P)$, respectively (25, 26). These transitions often split into three components because of the degeneracy left by the excited levels $^4T_1(P)$ and $^4T_1(F)$ by spin–orbit coupling and/or the John–Teller effect (24, 27). The band at 700 nm and the shoulder appearing between 400 and 550 nm are assigned to $^1A_{1g} \rightarrow {}^1T_{2g}$ and $^1A_{1g} \rightarrow {}^1T_{1g}$ transitions, respectively, of Co^{3+} ions (low spin) in an octahedral environment (28). They confirm the presence on the surface of TiO_2 of Co_3O_4, which is better described by a $[Co^{2+}]_{Td}[(Co^{3+})_2]_{Oh}O_4$ formula. The identification of octahedral Co^{2+} ions on the spectra is quite difficult because the absorption domains of Co^{2+} ions in Td and Oh symmetries overlap. Moreover, the absorption coefficient of tetrahedral Co^{2+} ions is quite superior to that of Co^{2+} ions in Oh symmetry.

The addition of small amounts of boron (0.2–0.5 wt%) to Co(7.6)/TiO_2 leads to a decrease in the intensity of the transitions $^1A_{1g} \rightarrow {}^1T_{2g}$ and $^1A_{1g} \rightarrow {}^1T_{1g}$ of the trivalent cobalt. Concomitantly, a shoulder attributed to Co^{2+} octahedral species which are characterized by ν_2 transitions located near 750 nm appears (29). The samples containing more boron (1–2 wt%) exhibit remarkable changes in their electronic spectra (Figs. 3d and 3e). The ν_1 and ν_2 transitions of Co^{3+} ions in octahedral sites disappear and the bands characteristic of Co^{2+} ions in tetrahedral sites centered on 540, 590, and 640 nm become much better resolved. Similar observations were made by Houalla and Delmon in studying the CoAlB system (30). On the other hand, it might be pointed out that the formation of Co–B mixed phases on the TiO_2 surface cannot be excluded, albeit such compositions were not identified by XRD analysis even at high loadings of cobalt and boron.

IR spectra. The modifications brought to the catalysts by boron addition were also studied by IR spectroscopy in the domain of B–O (2000–700 cm^{-1}) and O–H vibrations (3800–3000 cm^{-1}). The spectra recorded after evacuation of the samples for 1 h at 350°C are displayed in Figs. 4 and 5. The bands appearing between 1500 and 1150 cm^{-1} can be assigned to the valence vibrations of (BO_3) groups (31–35). These (BO_3) species also exhibit deformation vibrations that appear near 740 and 650 cm^{-1}. In the domain extending from 1150 to 900 cm^{-1}, it is the boron oxide B_2O_3that displays several absorptions, at 1120, 1070, and 940 cm^{-1}, due to valence vibrations of B–O in BO_4 tetrahedrons (31). These bands do not appear in the spectrum of H_3BO_3.

The spectrum of TiO_2 anatase (Fig. 4T) displays an intense band at 1370 cm^{-1} and a shoulder around 1260 cm^{-1} attributed to residual sulfate species left on the sample after its calcination (36). These sulfate species stabilize the TiO_2 anatase by preventing its transformation at high temperatures into the rutile phase, which leads to a less active catalyst in ethane ODH, even if the loaded quantity of cobalt is changed. They also enhance the acid properties of the carrier. Cobalt dispersion on TiO_2 (7.6%) does not affect the region of the spectrum where the $(SO_4)^{2-}$ groups appear (Fig. 4a), while boron addition to Co(7.6)/TiO_2 increases the intensity of some bands and favors the growth of several new ones, at 1320, 1270, 1235, 1130, and 1030 cm^{-1}. These bands broaden with the increase of boron content and reach a saturation for loadings superior to 1 wt% B. Boron species in a trigonal environment normally generate three bands, the most intense one being centered on

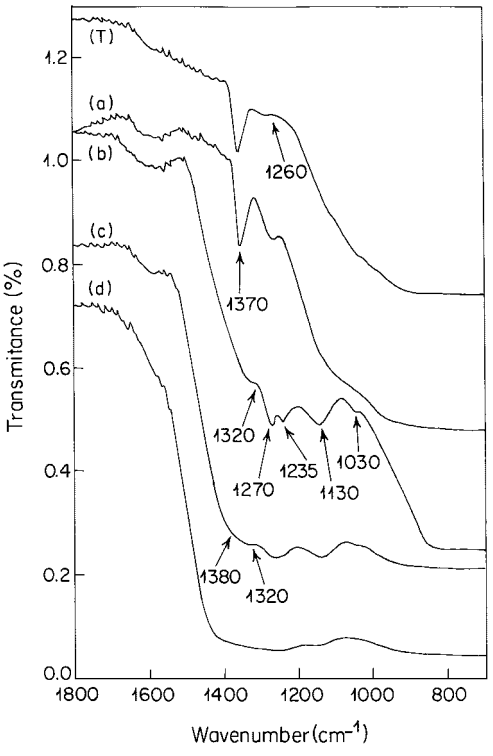

FIG. 4. IR (1800–700 cm^{-1}) spectra of B(x)Co(7.6)/TiO_2 recorded after evacuation at 350°C of (a) Co(7.6)/TiO_2, (b) B(0.25)Co(7.6)/TiO_2, (c) B(0.5)Co(7.6)/TiO_2, (d) B(1)Co(7.6)/TiO_2, and (T) TiO_2.

1300 cm^{-1}. However, these bands, according to Ramirez *et al.*, can shift toward low frequencies if boron interacts with the neighboring atoms (37). Aramendia and colleagues reported that this band appears at 1265 cm^{-1} if the vibrations of the B–O bond in a trigonal environment are affected by the adjacent cations (34). When boron is hosted by tetragonal sites, the B–O vibrations appear in the range 1200–1100 cm^{-1}. Therefore, as reported in the literature (31–35) and by comparison with the reference compounds, it might be concluded that the boron added to Co(7.6)/TiO_2 forms perhaps part of TiO_2 and is distributed between the trigonal and the tetragonal sites of the structure (34).

In the domain ranging from 4000 to 3000 cm^{-1} the spectrum of TiO_2 anatase exhibits only a broad band at 3665 cm^{-1} surrounded by two shoulders, near 3690 and 3631 cm^{-1}. Addition of cobalt and boron to TiO_2 gives rise, as shown in Fig. 5, to several new bands. The absorptions located at 3665 and 3631 cm^{-1} are due to weak acid OH groups bounded to Ti^{4+} ions that have different coordination numbers (31, 38). The shoulder at 3690 cm^{-1} can be ascribed to OH groups bonded to Ti^{4+} ions that interact with sulfate anions. Addition of cobalt (7.6 wt%) to TiO_2 suppresses the shoulder at 3690 cm^{-1} and concomitantly gives rise to a new band at 3735 cm^{-1}. This band was also observed on the MgO–CoO system and it was assigned to OH hydroxyls bonded to cobalt atoms. The band at 3665 cm^{-1} and the shoulder appearing around 3631 cm^{-1} can be attributed to OH groups of the carrier and/or to new OH groups belonging to the loaded active phase.

Addition of boron to Co(7.6)/TiO_2 (Figs. 5a–5d) resulted in the appearance of a band at 3690 cm^{-1} that increases with the loading increase. This band was also observed with B_2O_3/SiO_2, $B_2O_3/AlPO_4$, and B_2O_3/Al_2O_3 systems and was assigned to B–OH tetrahedrons (31, 39). The absorption at 3735 cm^{-1}, also found on the spectrum of Co(7.6)/TiO_2, disappeared after introducing 0.25 wt% B and a new one appeared around 3715 cm^{-1}. This band shifted toward high frequencies when the B content increased (3715–3744 cm^{-1}). New bands and significant modifications of the positions of their maxima occurred upon increasing boron loading (Figs. 5b–5d). Knozinger and Ratnasamy (40) Wachs (41) have reported that on alumina, the OH groups appearing at high frequencies have a basic character and their shift toward low frequencies can be associated with an increase in their acid character. Therefore, it might be concluded that boron addition to Co(7.6)/TiO_2 increased its surface acidity.

The acid–base properties of the catalysts were also investigated by adsorbing and desorbing 2,6-lutidine (2,6-dimethylpyridine) at different temperatures (Fig. 6). This probe molecule allows easy identification of acid sites on

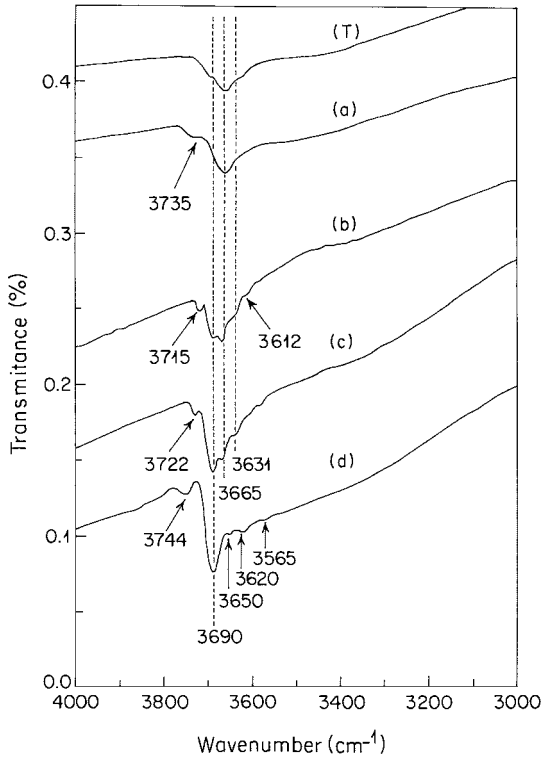

FIG. 5. IR (4000–3000 cm^{-1}) spectra of B(x)Co(7.6)/TiO_2 after evacuation at 350°C of (a) Co(7.6)/TiO_2, (b) B(0.25)Co(7.6)/TiO_2, (c) B(0.5)Co(7.6)/TiO_2, (d) B(1)Co(7.6)/TiO_2, and (T) TiO_2.

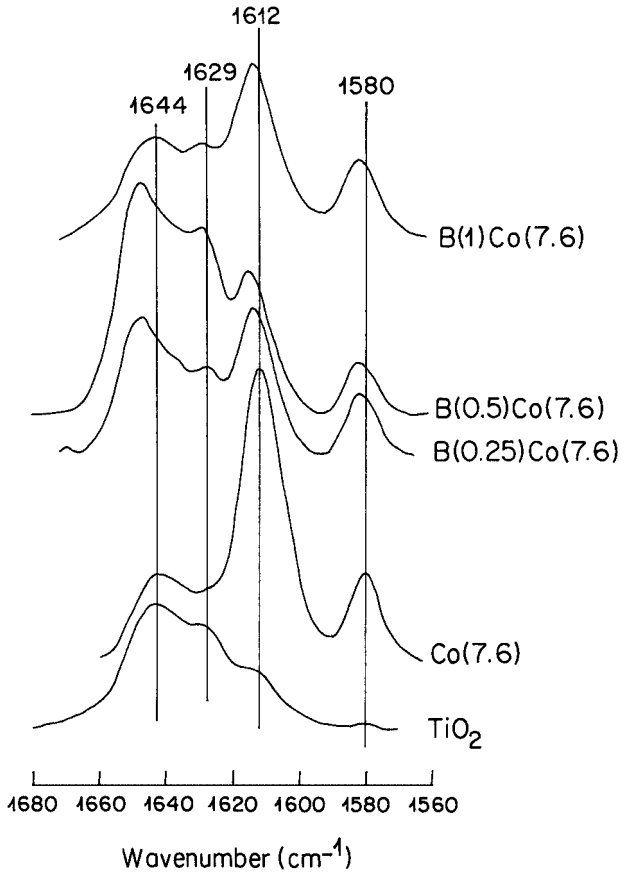

FIG. 6. Comparison of 2,6-lutidine IR spectra desorbed at 150°C from (a) $Co(7.6)/TiO_2$, (b) $B(0.25)Co(7.6)/TiO_2$, (c) $B(0.5)Co(7.6)/TiO_2$, (d) $B(1)Co(7.6)/TiO_2$, and (T) TiO_2.

a surface. It adsorbs on Brönsted acid sites, giving rise to two bands, near 1644 and 1628 cm^{-1} (BLu). The 2,6-lutidine coordinates also to Lewis acid sites (LLu), displaying two characteristic bands, located at 1612 and 1580 cm^{-1} (42–44). The Brönsted acid sites detected on TiO_2 free of any loading are probably due to OH hydroxyls bonded to sulfate groups. Introduction of cobalt increased the Lewis acidity and slightly decreased the Brönsted acidity. Figure 7 represents the changes that the acid sites densities underwent upon boron addition (Brönsted acidity = area of the bands at 1644 and 1628 cm^{-1}; Lewis acidity = area of the band at 1580 cm^{-1}). The density of Brönsted acidity increased with boron content and went through a maximum for a loading equal to 0.5 wt%. In the meantime, the Lewis acidity decreased, and after an addition of 0.5 wt% B it increased slowly. A shift toward high frequencies of the band at 1612 cm^{-1} (LLu) was also observed, indicating an increase in the strength of Lewis acidity.

3.2. Butan-2-ol Conversion

Butan-2-ol conversion was studied in order to underscore the effects of the catalyst acid–base properties on their activity in this reaction and in ethane ODH. This probe reaction allows the estimation of the surface acidity by investigating the catalyst dehydration and dehydrogenation abilities (45–47).

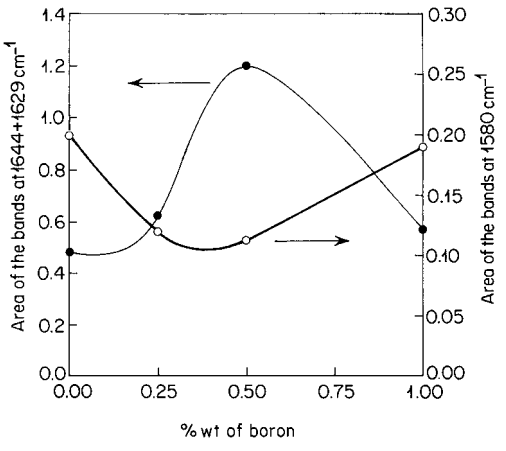

FIG. 7. Distribution of Lewis and Brönsted acidity versus boron content in $B(x)Co(7.6)/TiO_2$.

Figure 8 displays butan-2-ol conversion to butenes and butanone (methyl ethyl ketone) at stationary state in the absence of $O_2$from the reaction mixture. The nonimpregnated TiO_2 is slightly less active than $Co(7.6)/TiO_2$. Upon boron addition, the dehydration reaction increases rapidly and reaches a limit for a boron loading around 1 wt%. The dehydrogenation reaction is very weak and exhibits a maximum for 0.25 wt%. Beyond this concentration, it decreases to a negligible value. As previously reported, butan-2-ol dehydration requires acid sites whereas the dehydrogenation requests basic or redox sites (48). Usually, basic sites do not intervene in the dehydration process, and if they do,

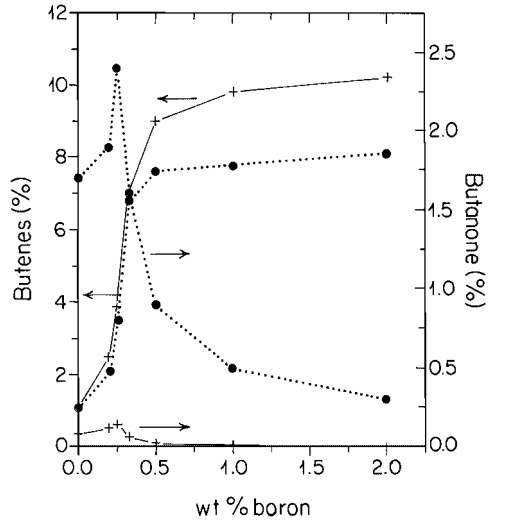

FIG. 8. Butan-2-ol conversion into butenes and butanone at 200°C versus boron content of $B(x)Co(7.6)/TiO_2$. (Solid line) Absence of O_2; (dotted line) presence of O_2.

TABLE 3

Activation Energies of Butan-2-ol Conversion over $B(0.25)Co(7.6)/TiO_2$ in Absence and Presence of O_2

Sample	Absence of oxygen		Presence of oxygen	
	E^a_{ene} (kJ)	E^a_{one} (kJ)	E^a_{ene} (kJ)	E^a_{one} (kJ)
$Co(7.6)/TiO_2$	128.9	80.2	140.2	79.1
$B(0.20)Co(7.6)/TiO_2$	120.8	73.5	122.2	67.4
$B(0.25)Co(7.6)/TiO_2$	107.3	73.1	111.2	62.8
$B(0.33)Co(7.6)/TiO_2$	88.3	86.5	92.4	77.7
$B(0.5)Co(7.6)/TiO_2$	78.5	89.8	82.8	81.8
$B(1)Co(7.6)/TiO_2$	71.2	92.5	76.2	83.8
$B(2)Co(7.6)/TiO_2$	70.3	95.6	72.6	87.2

they must be weaker than those involved in the dehydrogenation. Therefore, boron loadings superior to 0.25 wt% decrease notably the amount and the strength of the basic sites and subsequently the dehydrogenation activity. These results are in agreement with the modifications of the acid–base properties of the catalysts formerly investigated by IR spectroscopy using 2,6-lutidine adsorption.

The activation energy of the dehydration process (E^a_{ene}) (Table 3) decreases when boron content is increased, while for the dehydrogenation stage there is first a slight decrease, then an increase. These changes in energy reveal the modifications that occur on the catalyst surface upon boron introduction. The small maximum observed for the dehydrogenation reaction appears clearly as a minimum in the activation energies (E^a_{one}). Boron increases the catalysts acidity but concomitantly it decreases the number and strength of the basic sites. On the other hand, it also decreases the size of the Co_3O_4 particles and probably increases their dispersion.

The results obtained in the presence of air in the reaction mixture, at stationary state, are reported in Fig. 8. The dehydration activity undergoes the same changes as in the absence of O_2, albeit its limit is higher. Simultaneously, the dehydrogenation increases more than five times. The production of methyl ethyl ketone exhibits, surprisingly, as in the absence of oxygen, a maximum for a boron loading equal to 0.25 wt%, which suggests that the dehydrogenation reaction in both cases takes place on the same category of sites. Introduction of O_2 in the reaction mixture modifies the catalytic behavior of the catalyst surface. It adsorbs on the cobalt and produces O^{2-} basic specie, which enhance the performance of the dehydrogenation reaction (49) . For boron contents superior to 0.25 wt% the activity decreases rapidly. Boron becomes at these loadings a poison for the catalyst, probably because it spreads over the active sites, forming amorphous species. The activation energies determined at the stationary state for different B loadings in the presence of O_2 (Table 3) are inferior to those determined in the absence of oxygen.

3.3. Ethane ODH

The catalytic activity and selectivity of $B(x)Co(7.6)/TiO_2$ were also studied in ethane ODH reaction. Globally, the activity decreases, with time on stream, at all the reaction temperatures. It reaches a stationary state after 3 h on stream.

Figure 9 displays the ethane conversion and ethylene yield at stationary state and different boron loadings. All the curves have the same profile. At 550°C, the conversion reaches 28.4% with an ethylene yield of 19%. The best performance (maximum of conversion and C_2H_4 yield) is achieved for a boron content equal to 0.25 wt%. This addition of boron to $Co(7.6)/TiO_2$ increases its activity from 22 to 28.4% and the ethylene yield from 13 to 19%. Above

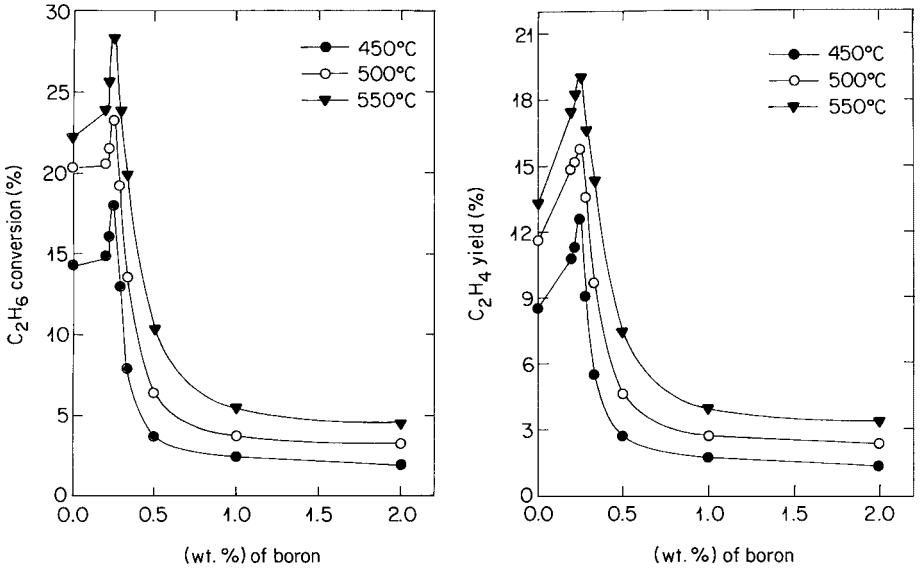

FIG. 9. Ethane conversion (α_g) and ethylene yield (η_{ene}) versus boron content at different temperatures over $B(x)Co(7.6)/TiO_2$.

this loading, as in the case of butan-2-ol dehydrogenation, the catalyst performance decreases abruptly. It is, however, worth pointing out that unexpectedly the sharp maximum of activity observed here coincides with that obtained with butan-2-ol, for the same boron content (Fig. 9).

Previous studies have shown that supported vanadia is one the most active and selective catalysts, with a conversion and a selectivity approaching 30 and 60%, respectively. This good performance is often related by the authors to the redox properties of VO_x species (50). The B(0.25)Co(7.6)/TiO_2 exhibits a comparable activity at the same reaction temperatures. This catalyst is also of value in understanding the fundamental aspects of catalysis, since it does not own conventional redox centeres but is active in oxidative dehydrogenation processes. On the other hand, this system has barely been studied in oxidant atmospheres such as those investigated here.

Its well known that the selectivity depends considerably on the extent of the conversion. Therefore, in order to properly compare the performances of the catalysts, experiments were performed to determine their selectivity at the same conversion. Figure 10 displays the results and confirms that the best performance is exhibited by B(0.25)Co(7.6)/TiO_2.

The investigation of the catalysts behavior also showed that their activity and selectivity do not depend on the method of preparation. The use of catalysts synthesized by sequential impregnation (Co(7.6)/B(0.25)/TiO_2) leads to approximately the same results as those obtained using coimpregnated catalysts (B(0.25)Co(7.6)/ TiO_2). This is probably because regardless of the sequence of Co and B introduction, cobalt is in excess and seems to always occupy on TiO_2 the same sites. The quantity loaded (7.6 wt%) exceeds the amount needed for the completion of the monolayer. Boron addition, independent of its method of introduction, always leads to amorphous mixed phases similar to those described in the literature for $MgO–B_2O_3$ prepared by coprecipitation (B, Mg, and Co possess comparable ionic radii) (34).

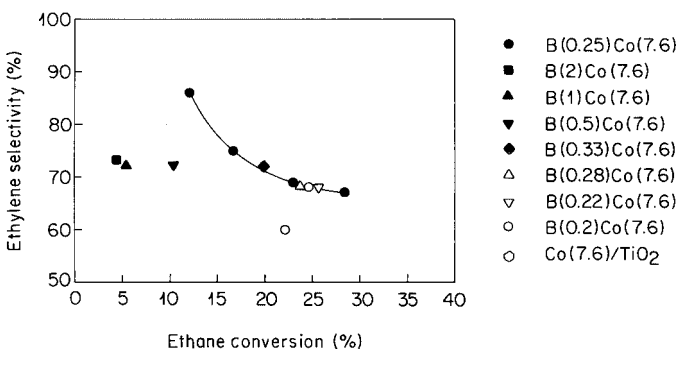

FIG. 10. Variation of ethylene selectivity (S_{ene}) versus the conversion (α_g) at 550°C.

TABLE 4

X-Ray Identification of the Phases after Catalytic Tests

Sample	Identified phases
Co(7.6)/TiO_2	TiO_2 anatase + Co_3O_4 + $CoTiO_3$ + Co_2TiO_4
B(0.25)Co(7.6)/TiO_2	TiO_2 anatase + Co_3O_4 + $CoTiO_3$ + Co_2TiO_4
B(0.33)Co(7.6)/TiO_2	TiO_2 anatase + Co_3O_4 + $CoTiO_3$ + Co_2TiO_4
B(0.5)Co(7.6)/TiO_2	TiO_2 anatase + Co_3O_4 + $CoTiO_3$ + Co_2TiO_4
B(1)Co(7.6)/TiO_2	TiO_2 anatase
B(2)Co(7.6)/TiO_2	TiO_2 anatase

3.4. Characterizations after Tests

The catalyst color was observed to change throughout the tests from brown-grey to green. This modification of color can be related to an alteration of cobalt coordination subsequent to the formation of well-defined phases and Co^{3+} reduction into Co^{2+} ions. The decay of activity observed in the first 3 h of reaction could also be, at least in part, attributed to these changes. In order to trace them, characterization of the catalysts after the catalytic tests were performed. As Table 1 illustrates, the specific surface areas of the samples decreased after the tests. Table 1 also shows that large amounts of boron minimize this decrease.

XRD patterns. X-ray diffraction patterns of the B(x)Co(7.6)/TiO_2 recorded after the runs show that the anatase phase did not undergo any crystallographic change at the investigated reaction temperatures, probably because initially it contained sulfates that stabilize its structure (Table 4). Besides Co_3O_4, which appears after the sample calcination, two new phases were identified as being $CoTiO_3$ (JCPDS 77-1373) and Co_2TiO_4 (JCPDS 39-1410). In $CoTiO_3$, Ti^{4+} and Co^{2+} are hosted by slightly distorted octahedral sites (51). Co_2TiO_4 is an inverse spinel and is better represented by a $(Co^{2+})_{Td}(Co^{2+}Ti^{4+})_{Oh}O_4$ formula in which half of the Co^{2+} ions occupy tetrahedral sites. The other half and the Ti^{4+} ions are in octahedral sites (52). The formation of these phases is possibly promoted by the reducing character of the reaction mixture despite the fact that it contains O_2. For boron loadings inferior to 1 wt%, XRD spectra are not affected, whereas for superior quantities the peak width increases and the formation of $CoTiO_3$ and Co_2TiO_4 is completely inhibited.

UV–visible NIR spectroscopy. The DRS spectra of B(x)Co(7.6)/TiO_2 recorded after catalytic tests (Fig. 11) reveal that in comparison with the initial samples (Fig. 3) several differences appear in the visible and NIR domains. The shoulder located between 400 and 550 nm and the band centered on 700 nm are characteristic of Co_3O_4. The three peaks at about 630, 590, and 540 nm are due to $^4A_2(F) \rightarrow {}^4T_1(P)$ transition of Co^{2+} ions in tetrahedral sites. There is also, near 760 nm, a shoulder which is overlapped by the band at 700 nm. This shoulder was, before the tests,

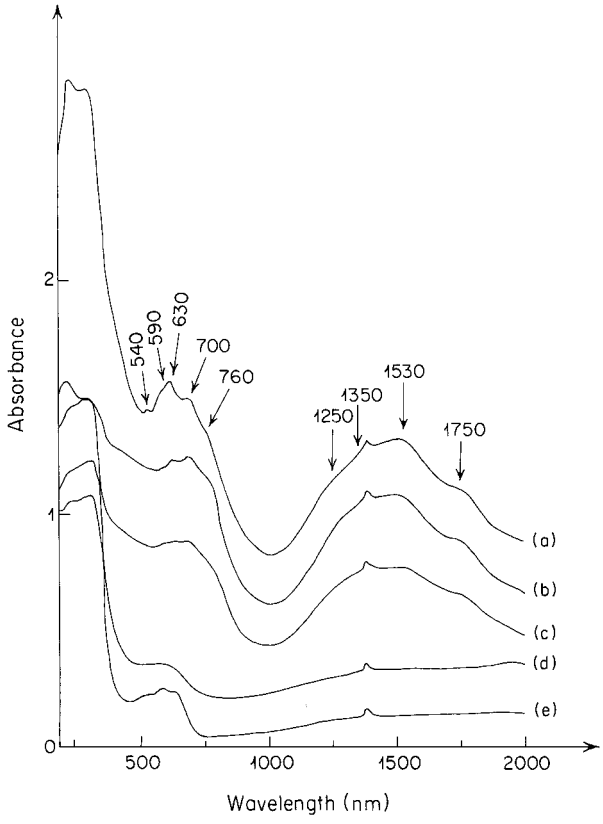

FIG. 11. DR spectra of B(x)Co(7,6)/TiO_2 recorded after catalytic runs: (a) Co(7.6)/TiO_2, (b) B(0.25)Co(7.6)/TiO_2, (c) B(0.5)Co(7.6)/TiO_2, (d) B(1)Co(7.6)/TiO_2, (e) B(2)Co(7.6)/TiO_2.

absent from the spectra of the samples containing more than 1 wt% B. In the near-infrared region, a new band assigned to $^4A_2$ (F) $\rightarrow$ $^4T_1$(F) transition appears near 1750 nm.

In order to confirm the attribution of the bands that arise after the runs and to relate their appearance to the formation of new phases, $CoTiO_3$ and Co_2TiO_4 were synthesized. These bands are listed in Table 5 and compared with those of reference compounds. Co_2TiO_4 exhibits (i) a broad absorption spreading over 1300–1820 nm and three absorptions near 670, 623, 580 nm that can be assigned to ν_1 and ν_2 transitions of Co^{2+} in tetrahedral sites, respectively (53); (ii) three shoulders, around 535, 720, and 1150 nm, that are assigned to the transitions ν_1, ν_2, and ν_3 of Co^{2+} ions in octahedral sites (29). The spectrum of the ilmenite $CoTiO_3$ phase is similar to that of $(CoCl_6)^{4-}$ and Co_2SiO_4. It is mainly characterized by three bands, located at 600, 760, and 1530 nm (29). The spectra of the catalysts after the tests contain bands belonging to $CoTiO_3$ and Co_2TiO_4 phases. Therefore, the shoulder at 760 nm can be ascribed to Co^{2+} ions hosted by the octahedral sites of the ilmenite phase and the band at 1750 nm to Co^{2+} ions in the tetrahedral sites of the spinel Co_2TiO_4. The spectra of the samples containing more 1 wt% B do not show any noticeable modification compared to those of the initial samples loaded with the same boron amounts. At high concentrations boron totally inhibits the formation of $CoTiO_3$ and Co_2TiO_4. It was previously shown that these phases are less active and less selective than Co(7.6)/TiO_2 in ethane ODH. Their formation produces a decrease in the catalyst surface area and a reduction of Co^{3+} ions into Co^{2+} (13).

Besides the crucial role played by the structural properties of the catalyst surface, several authors reported that the acid–base properties intervene in the ODH processes. Concepcion *et al.*, in investigating a series of vanadium-based catalysts, reported that the olefin selectivity depends on the acid–base features of the catalysts and on the nature of the hydrocarbon used (54). Grabowski *et al.* (7) showed that alkali introduction into VO/TiO_2 and MoO_3/TiO_2 systems increases their olefin selectivity. It was also observed, in agreement with the results presented here, that boron addition to alumina improves its performances in the same class of reactions (12). The importance of these acid–base properties

TABLE 5

UV–Visible–NIR Band Positions (in nm) and Assignments of Cobalt Ions in B(x)Co(7.6)/TiO_2 Catalysts and Reference Compounds

	Co^{2+} (Td)		Co^{2+} (Oh)			Co^{3+} (Oh)	
Sample	ν_1 $^4A_2 \rightarrow {}^4T_1$ (F)	ν_2 $^4A_2 \rightarrow {}^4T_1$ (P)	ν_1 $^4T_{1g} \rightarrow {}^4T_{2g}$ (F)	ν_2 $^4T_{1g} \rightarrow {}^4A_{2g}$ (F)	ν_3 $^4T_{1g} \rightarrow {}^4T_{1g}$ (P)	ν_1 $^1A_{1g} \rightarrow {}^1T_{1g}$	ν_2 $^1A_{1g} \rightarrow {}^1T_{2g}$
Low-boron-content BCo/TiO_2	1750, 1530, 1350, 1250	630, 590, 540	sh. 760			700	420
			ν_1 and ν_3 are weak because the extinction coefficients of the bands of Co^{2+} (Td) are higher than those of Co^{2+} (Oh)				
High-boron-content BCo/TiO_2	Very weak	640, 590, 540	Contain only Co^{2+} in tetrahedral symmetry				
Co_2TiO_4	1820–1300	670, 623, 580	sh. 1150	sh. 720	sh. 535	Contains 50% Co^{2+} in Oh symmetry and 50% Co^{2+} in Td symmetry	
$CoTiO_3$	Contains only Co^{2+} in octahedral symmetry		1530	760	596	Contains only Co^{2+} in octahedral symmetry	

is also illustrated by the maximum observed in butan-2-ol dehydrogenation (in the presence and absence of O_2 in the reaction mixture), which coincides with that observed in ethane ODH for the same boron loading (0.25 wt%). This result suggests, as pointed out above, that both reactions involve similar active sites and require the same ratio of Brönsted and Lewis acid centeres to exhibit the best activity and selectivity. As a result, when the catalyst is overloaded with boron, the acidity increases too much and provokes a marked decrease in butan-2-ol dehydrogenation as well as a loss of activity and selectivity in ethane ODH.

4. CONCLUSION

From the presented results the following conclusions can be drawn.

- Cobalt-loaded titanium dioxide $Co(7.6)/TiO_2$ is active in ethane ODH. Its activity decreases from 33% to reach, after 3 h on stream, a stationary state characterized by a conversion of 22% and a selectivity of 60%. Throughout the transitory state of activity, the specific surface area decreases and concomitantly a formation of less selective $CoTiO_3$ and Co_2TiO_4 phases was observed.
- Addition of boron to $Co(7.6)/TiO_2$ changes notably the catalyst acid–base properties. Butan-2-ol confirmed these results and showed that the best performance is achieved when boron content equals 0.25 wt%. The dehydrogenation reaction (in the presence and in the absence of oxygen) exhibits a maximum for that loading.
- In the ethane ODH reaction, addition of boron to $Co(7.6)/TiO_2$ improves the catalytic performances. A maximum of conversion (at stationary state) equal to 28% with an ethylene selectivity of 67% was achieved for a boron loading of 0.25 wt%. For the same loading, a similar maximum was observed in butan-2-ol dehydrogenation, suggesting that both reactions take place on the same active sites. The activity improvement subsequent to boron introduction was related, as shown by XRD and HRTEM analyses, to the decrease in the size of Co_3O_4 crystallites and to the optimization of the surface acid–base properties by the introduction of 0.25 wt% boron.

ACKNOWLEDGMENTS

The authors are indebted to the French Ministry of Foreign Affaires for the financial support provided (Action Intégrée 183/MA/99). The ITODYS laboratory (Université Paris 7-Denis Diderot) is gratefully acknowledged for the LRS analysis. The help of M. Potvin (laboratoire de Réactivité de Surface, Université Pierre et Marie Curie) in XRD measurements was also greatly appreciated.

REFERENCES

1. Centi, G., and Trifiro, F., *Catal. Today* **3**, 151 (1988).
2. Thorsteinson, E. M., Wilson, T. P., Young, F. G., and Kasai, P. H., *J. Catal.* **52**, 116 (1978).
3. Dai, H. X., Au, C. T., Chan, Y., Hui, K. C., and Leung, Y. L., *Appl. Catal. A* **213**, 91 (2001).
4. Michalakos, P. M., Kung, M. C., Jahan, I., and Kung, H. H., *J. Catal.* **140**, 226 (1993).
5. Aaddane, A., Kacimi, M., and Ziyad, M., *Catal. Lett.* **73**, 47 (2001).
6. Essayem, N., Gayraud, P.-Y., Coudurier, G., Védrine, J. C., Habermarcher, D., Sassi, A., and Sommer, J., *J. Catal.* **183**, 292 (1999).
7. Grabowski, R., Grzybowska, B., Samson, K., Sloczynsky, J., Stoch, J., and Wcislo, K., *Appl. Catal. A* **125**, 129 (1995).
8. Tessier, L., Bordes, E., and Gubelmann-Bonneau, M., *Catal. Today* **24**, 335 (1995).
9. El-Drissi, J., Kacimi, M., Loukah, M., and Ziyad, M., *J. Chim. Phys.* **94**, 1984 (1997).
10. El-Drissi, J., Kacimi, M., Bozon-Verduraz, F., and Ziyad, M., *Catal. Lett.* **56**, 221 (1998).
11. Colorio, G., Védrine, J. C., Auroux, A., and Bonnetot, B., *Appl. Catal. A* **137**, 55 (1996).
12. Murakami, Y., Otsuka, K., Wada, Y., and Morikawa, A., *Chem. Lett.* 535 (1989).
13. Brik, Y., Kacimi, M., Ziyad, M., and Bozon-Verduraz, F., *J. Catal.* **202**, 118 (2001).
14. Xu, B., Dong, L., and Chen, Y., *J. Chem. Soc. Faraday Trans.* **94**(13), 1905 (1998).
15. Li, J., and Coville, N. J., *Appl. Catal. A* **181**, 201 (1999).
16. Baertsch, C. D., Komala, K. T., Chua, Y.-H., and Iglesia, E., *J. Catal.* **205**, 44 (2002).
17. Stanick, M. A., Hoalla, M., and Hercules, D. M., *J. Catal.* **104**, 396 (1987).
18. Ohsaka, T., Izumi, F., and Fujiki, Y., *J. Raman Spectrosc.* **7**, 321 (1978).
19. Stanick, M. A., Hoalla, M., and Hercules, D. M., *J. Catal.* **106**, 362 (1987).
20. Jezlorowski, H., Knozinger, H., Krange, P., and Gajardo, P., *J. Phys. Chem.* **84**, 1825 (1980).
21. Hibben, J., "The Raman Effect and Its Chemical Applications." Reinhold, New York, 1939.
22. Roy, M., Ponceblanc, H., and Volta, J. C., *Top. Catal.* **11/12**, 101 (2000).
23. Morales, A. B., Novaro, O., Lopez, T., Sanchez, E., and Gomez, R., *J. Mater. Res.* **10**, 2788 (1995).
24. Verberckmoes, A., Weckhuysen, B. M., and Schoonheydt, R. A., *Microporous Mesoporous Mater.* **22**, 165 (1998).
25. Jacono, M. L., and Cimino, A., *Gazz. Chim. Ital.* **103**, 1281 (1973).
26. Pappalardo, R., Wood, D. L., and Linares, R. C., *J. Chem. Phys.* **35**, 2041 (1961).
27. Lever, A. B. P., "Inorganic Electronic Specroscopy." Elsevier, Amsterdam/New York 1984.
28. Noronha, F. B., Perez, C. A., Schmal, M., and Fréty, R., *Phys. Chem. Chem. Phys.* **1**, 2861 (1999).
29. Goodgame, M., and Cotton, F. A., *J. Phys. Chem.* **85**, 791 (1961).
30. Houalla, M., and Delmon, B., *Appl. Catal. A* **1**, 285 (1981).
31. Bautista, F. M., Campelo, J. M., Garcia, A., Luna, D., Marinas, J. M., Moreno, M. C., Romero, A. A., Navio, J. A., and Macias, M., *J. Catal.* **173**, 333 (1998).
32. Laperches, J. P., and Tarte, P., *Spectrochim. Acta* **22**, 1201 (1966).
33. Ross, S. D., *Spectrochim. Acta* **28A**, 1555 (1972).
34. Aramendia, M. A., Borau, V., Jiménez, C., Marinas, J. M., Porras, A., and Urbano, F. J., *J. Mater. Chem.* **3**, 819 (1999).
35. Mazza, D., and Vallino, M., *J. Am. Ceram. Soc.* **75**(7), 1929 (1992).
36. Mortera, C., Chiorino, A., and Zecchina, A., *Gazz. Chim. Ital.* **109**, 691 (1979).
37. Ramirez, J., Castillo, P., Cedeno, R., Castillo, M., Palacios, J. M., and Lopez-Agudo, A., *Appl. Catal. A* **132**, 317 (1995).
38. Mortera, C., *J. Chem. Soc. Faraday Trans.* **84**(5), 1617 (1988).
39. Mortera, C., and Low, M. J. D., *J. Phys. Chem.* **74**, 1297 (1970).
40. Knozinger, H., and Ratnasamy, P., *Catal. Today* **27**, 497 (1996).

41. Wachs, I. E., *Catal. Today* **27**, 437 (1996).
42. Matulewicz, E. R. A., Kerkhof, F. P. J. M., Moulijn, J. A., and Reitsma, H. J., *J. Colloid Interface Sci*. **70**, 209 (1979).
43. Miyata, H., and Moffat, J. B., *J. Catal*. **62**, 357 (1980).
44. Berhault, G., Lacroix, M., Breysse, M., Maugé, F., Lavalley, J. C., Nie, H., and Ou, L., *J. Catal*. **178**, 555 (1998).
45. Aramendia, M. A., Borau, V., Jiménez, C., Marinas, J. M., Porras, A., and Urbano, F. J., *J. Catal*. **161**, 829 (1996).
46. Godard, E., Gaigneaux, E. M., Ruiz, P., and Delmon, B., *Catal. Today* **61**, 279 (2000).
47. Benarafa, J., Kacimi, M., Coudurier, G., and Ziyad, M., *Appl. Catal. A* **196**, 25 (2000).
48. Kacimi, M., and Ziyad, M., *J. Chim. Phys*. **94**, 2007 (1997).
49. Giamello, E., Sojka, Z., Che, M., and Zecchina, A., *J. Phys. Chem*. **90**, 6084 (1986).
50. Argyle, M. D., Chen, K., Bell, A. T., and Iglesia, E., *J. Catal*. **208**, 139 (2002).
51. Newnham, R. E., Fang, J. H., and Santoro, R. P., *Acta Cristallogr.* **17**, 240 (1964).
52. Gulabshankar, D. R., and Vishnu, D. S., *Bull. Chem. Soc. Jpn*. **64**, 2449 (1991).
53. Bizi, M., Ph.D. thesis. University of Rouen, France, 1989.
54. Concepcion, P., Galli. A., and Lopez Nieto, J. M., *Top. Catal*. **3**, 451 (2000).